

Article

Research on the Bonding Performance of BFRP Bars with Reactive Powder Concrete

Jie Xiao ¹, Yikang Murong ¹, Xiyuan Chen ¹, Lingfei Liu ², Keyi Zhai ³, Haibo Jiang ^{1,*}, Linhai Huang ¹ and Guodong Wang ¹

¹ School of Civil and Transportation Engineering, Guangdong University of Technology, Guangzhou 510006, China; xiaojie2017@gdut.edu.cn (J.X.); 2112109015@mail2.gdut.edu.cn (Y.M.); 2112109142@mail2.gdut.edu.cn (X.C.); 3119002837@mail2.gdut.edu.cn (L.H.); 3121002901@mail2.gdut.edu.cn (G.W.)

² School of Transportation, Civil Engineering & Architecture, Foshan University, Foshan 528225, China; lingfeiliu@fosu.edu.cn

³ Guangxi Tianxin Expressway Co., Ltd., Nanning 530022, China; 2111909042@mail2.gdut.edu.cn

* Correspondence: hbjiang@gdut.edu.cn

Abstract: In recent years, replacing steel bars with basalt fiber-reinforced polymer (BFRP) bars and replacing ordinary concrete with reactive powder concrete (RPC) are considered effective solutions to the corrosion problem of steel bars in ordinary reinforced concrete structures. In order to study the bonding performance between BFRP bars and RPC, a total of 27 bonding specimens were tested by pull-out test. The effects of steel fiber volume content (0%, 1.5%, 2%), protective layer thickness (25 mm, 40 mm, 55 mm, 69 mm), and bond anchorage length of bars (3 d, 4 d, 5 d; d is the diameter of the bars) on the bond performance were studied. The experimental results indicated that the BFRP bar and reactive powder (RPC) concrete interface exhibited better bonding performance, and the steel fibers mixed in RPC can play the role of crack-blocking enhancement in the specimen, which improves the shear and tensile properties of the concrete, thus improving the bond strength between BFRP bar and RPC. Three failure modes were observed in the pull-out tests: BFRP bar shear failure, splitting failure, and concrete shear failure. The bond strengths of BFRP bars and RPC with 0%, 1.5%, and 2% steel fiber content were 24.2 MPa, 32.1 MPa, and 34.5 MPa, respectively. With the increase in bond anchorage length, the ultimate bond strength tended to increase first and then decrease. There may be an optimal bonding length between BFRP bar and reactive powder concrete, and when the optimal bonding length is exceeded, the bond strength decreases with the increase in bonding length. With the increase in the protective layer thickness, the improvement in the bond strength of the BFRP bar and RPC was not very significant.

Keywords: BFRP bars; reactive powder concrete; pull-out tests; bonding performance



Citation: Xiao, J.; Murong, Y.; Chen, X.; Liu, L.; Zhai, K.; Jiang, H.; Huang, L.; Wang, G. Research on the Bonding Performance of BFRP Bars with Reactive Powder Concrete. *Buildings* **2023**, *13*, 2083. <https://doi.org/10.3390/buildings13082083>

Academic Editor: Mohamed K. Ismail

Received: 12 July 2023

Revised: 9 August 2023

Accepted: 15 August 2023

Published: 16 August 2023



Copyright: © 2023 by the authors. Licensee MDPI, Basel, Switzerland. This article is an open access article distributed under the terms and conditions of the Creative Commons Attribution (CC BY) license (<https://creativecommons.org/licenses/by/4.0/>).

1. Introduction

Reinforced concrete structures have been the most widely used structures in civil engineering since the late 19th century due to good mechanical properties, low cost, and good durability in normal environments [1–4]. However, under corrosive environmental conditions (such as marine environment, deicing salt environment, carbonation environment, acid corrosion environment, etc.), the steel bars in reinforced concrete structures are prone to corrosion, resulting in cracking and peeling of the concrete. Steel bar corrosion is one of the main causes of performance deterioration of concrete structures, significantly affecting their structural performance [5–9]. In recent years, the use of fiber-reinforced polymer composite (FRP) bars, replacing steel bars, has been considered an effective solution to the problem of steel bar corrosion [10–13]. Compared with steel bars, FRP bars have the advantages of high tensile strength, corrosion resistance, light weight, electrical insulation, and fatigue resistance [14,15]. At present, FRP bars applied in civil engineering

structures mainly include glass fiber-reinforced polymer composite bars (GFRP), carbon fiber-reinforced polymer composite bars (CFRP), basalt fiber-reinforced polymer composite bars (BFRP), and aramid fiber-reinforced polymer composite bars (AFRP). Among them, BFRP reinforcement usually has better mechanical properties and chemical stability than GFRP reinforcement, and its price is much lower than CFRP reinforcement [16,17]. Furthermore, basalt fibers are materials made from the original volcanic rock. The preparation process for basalt fibers does not produce other harmful substances and is environmentally friendly. They have excellent comprehensive performance and optimistic development prospects and have become a hot research topic both domestically and internationally in recent years [18]. In addition, researchers have developed a cementitious composite material with high strength, toughness, and durability, namely reactive powder concrete (RPC), to improve the durability of the reinforced concrete structure itself. RPC is based on the closest packing theory, using fine quartz sand as the aggregate and adding steel fibers and high-efficiency water-reducing agents to reduce the internal pores and micro-fractures of the material [19–21]. Therefore, it has better flexural strength, compressive strength, and corrosion resistance than ordinary concrete and has broad application prospects in engineering.

The research literature on the bonding performance of BFRP and different types of concrete is relatively abundant. Wang et al. [22] investigated the synergistic effect of sustained load and seawater sea-sand concrete (SWSSC) environment on the degradation of GFRP and BFRP bars. Xiong et al. [23] paid attention to the bonding behavior between recycled aggregate concrete (RAC) and basalt fiber-reinforced polymer (BFRP) bars, and they found that the bond strength increased with the concrete strength. Trabacchin et al. [24] conducted pull-out tests to study the bonding behavior of basalt fiber-reinforced polymer (BFRP) bars in geopolymer concrete (GPC), and they found that the chemical adhesion was low, and the bond was mainly dependent on mechanical interlocking. Ahmed et al. [25] carried out pullout tests under monotonic and cyclic loading patterns to examine the effect of cyclic loading on the bonding behavior of BFRP bars, and their results revealed that cyclic loading had a significant effect on the bonding performance of BFRP bars. Henin et al. [26] evaluated the effect of two surface conditions (primary sand coating and secondary sand coating) on the bonding of BFRP bars in concrete, and they found that the surface condition of BFRP bars had a significant effect on the bond strength, bond-dependent coefficient, and flexural strength. Dai et al. [27] carried out a pull-out test to investigate the interfacial bonding behavior between seawater sea-sand concrete (SSWSC) and BFRP bars, and they found that decreasing the diameter of BFRP bars and increasing the concrete protective layer thickness were beneficial for improving bond strength. Chen et al. [28] studied the dynamic bonding performance of BFRP bar-to-concrete interfaces by pull-out tests, and the results showed that increasing the concrete strength and the loading rates would improve the bond strength. Lu et al. [29] studied the bond durability of basalt fiber reinforced polymer (BFRP) bars and concrete with or without fly ash in corrosion environments via pull-out tests, and they found that with the prolongation of immersion time, the mechanical properties and bond strength of BFRP bars decreased. Sun et al. [30] analyzed the bonding behavior between basalt fiber-reinforced polymer (BFRP) bars and 3D printed concrete by pull-out tests, and the results indicated that the bond strength of 3D printed specimens was smaller than that of conventional mold-cast specimens and that the bond strength between 3D printed specimens and sand-coated BFRP bars was larger than the bond strength between 3D printed specimens and smooth BFRP bars. The studies on the bonding performance of reactive powder concrete (RPC) –steel bar are also relatively sufficient. Wang et al. [31] reported eccentric pull-out tests to investigate the bond–slip behavior between reactive powder concrete (RPC) and reinforcing bars, and the results showed that the order of factors influencing bond strength from strong to weak were bond length, concrete strength, protective layer thickness, and steel bar diameter. Piccinini et al. [32] studied the bonding behavior of steel bars and reactive powder concrete (RPC), with 35% cement replaced by blast furnace slag, and the results indicated that the bond strength

between plain round steel bars and RPC was 20% lower than that between ribbed steel bars and RPC. Bae et al. [33] employed the direct pull-out test method to study the bond stress between conventional reinforcement and steel-fiber-reinforced reactive powder concrete (SFRPC); they observed that the ultimate bond stress between steel bars and RPC mixed with 1% volume fraction of steel fibers was twice as much as that of a regular RPC matrix without steel fibers. However, adding 2% volume fraction of steel fibers did not significantly increase the ultimate bond stress between RPC and steel bars.

If reactive powder concrete (RPC) and basalt fiber-reinforced polymer composite bars (BFRP) are replaced with concrete and steel bars in traditional reinforced concrete structures, the excellent mechanical properties and corrosion resistance of RPC and BFRP bars can be fully utilized. The bonding and anchoring performance between steel bars and concrete in traditional reinforced concrete structures is a prerequisite for working together. Similarly, a key indicator for evaluating the structural performance of BFRP-reinforced reactive powder concrete structures is the bond strength between the BFRP bars and reactive powder concrete. The excellent bonding properties between BFRP bars and concrete are the premise for ensuring the stress transfer at the interface between them and the guarantee for their cooperation in resisting deformation and bearing the load. The production process, surface shape and mechanical properties of BFRP bars are different from those of ordinary steel bars, and the existing research on the bonding properties of ordinary steel bars cannot be directly applied to BFRP bars. At the same time, the mechanical properties of reactive powder concrete (RPC) are significantly different from those of high-strength concrete and ordinary steel fiber concrete, so the existing research results on the bonding properties of high-strength concrete and ordinary steel fiber concrete are no longer applicable [7]. Therefore, it is necessary to investigate the bonding performance of BFRP bars and reactive powder concrete (RPC).

In this study, an experimental study on bonding performance between reactive powder concrete (RPC) and BFRP bars was conducted using a pull-out test. The test parameters included fiber volume content, protective layer thickness, and bond anchorage length of bars to reveal the bond–slip damage pattern between them and the influence of the above three variables on their performance. At the same time, the bond failure and cracking pattern and damage mechanism of BFRP bars in plain concrete and reactive powder concrete were compared to provide some experimental basis for improving the bond–slip theory of reactive powder concrete and BFRP bars.

2. Experiment Design and Test Methods

2.1. Experiment with Material Design

The cement adopted was P II 52.5 Portland cement. Silica fume was produced by a factory in Zhejiang province with a particle size of less than 1 μm . Fine aggregate used high-quality fine sand with a particle size passing through a 1.18 mm aperture sieve. Fiber used RS65113-2850 hooked-end steel fiber, and the water-reducing agent was a polycarboxylic acid type high-efficiency water-reducing agent with a water reduction rate of 20%. The compressive standard size of the RPC cube was 100 mm \times 100 mm \times 100 mm. The compressive strength cube specimens of reactive powder concrete (RPC) and ordinary concrete were cast and cured under the same conditions, and the measured compressive strengths of RPC and ordinary concrete with 0, 1.5% and 2% steel fibers were 78.3 MPa, 99.7 MPa, 117.1 MPa and 43.2 MPa, respectively. In this study, the constituent materials of reactive powder concrete (RPC) and ordinary concrete were as listed in Table 1.

Table 1. Concrete mix design.

Materials/kg/m ³	Ordinary Concrete	Steel Fiber Content of Reactive Powder Concrete (RPC)/%			
		0	1	1.5	2
Sand	640	1021	1021	1021	1021
Gravel	1138	–	–	–	–
Water	217	191	191	191	191
Cement	368	827	827	827	827
Silica fume	–	203	203	203	203
Calcium carbonate	–	33	33	33	33
Steel fiber	–	–	78	116	156
Water reducer	–	27	27	27	27

The FRP bars were threaded basalt fiber-reinforced polymer (BFRP) bars with a nominal diameter of 12 mm. Five samples of BFRP bars were randomly selected for mechanical properties testing by referring to a Chinese standard “Test method for basic mechanical properties of fiber reinforced polymer bar” (GB/T 30022-2013) [34]. Due to the low shear strength of BFRP bars, 200 mm long seamless steel pipes were placed and anchored with epoxy resin adhesive in the loading part of the BFRP bars before the test to prevent failure of the BFRP bars at the loading end when testing the tensile strength of BFRP bars. The measured modulus of elasticity of BFRP bars was 52.6 GPa, and the tensile strength was 1210 MPa. The steel bars in this study were HRB400 grade steel bars with 12 mm diameter, and the ultimate tensile strength was 625 MPa. The BFRP bars used in the tests were threaded bars with no special surface treatment, as shown in Figure 1.

**Figure 1.** BFRP bar tensile test.

2.2. Test Design

The pull-out specimen was designed as a 150 mm × 150 mm × 150 mm cube specimen, as shown in Figure 2. The test specimen was molded by a wooden template with a 20 mm diameter circular hole in the center of two parallel templates, one of which was pierced with a PVC pipe of a certain length to prevent the concrete from being crushed by the pressurized steel plate at the loading end, and the other end was equipped with a pipe

cap in the center of the template to ensure the flatness of the specimen. The free end was reserved by 30 mm to measure the relative slip between the free end and the concrete surface, as shown in Figure 3. A seamless steel pipe of 150 mm in length was inserted to prevent the loading equipment from damaging the surface of the FRP bars during the loading process. The diameter of the steel pipe was 4–6 mm larger than that of the FRP bars, and the gap between the steel pipe and the FRP bars was filled with epoxy resin glue; the bonding length of the FRP bars was adjusted by changing the length of the PVC pipe.



Figure 2. Specimen wooden molds.

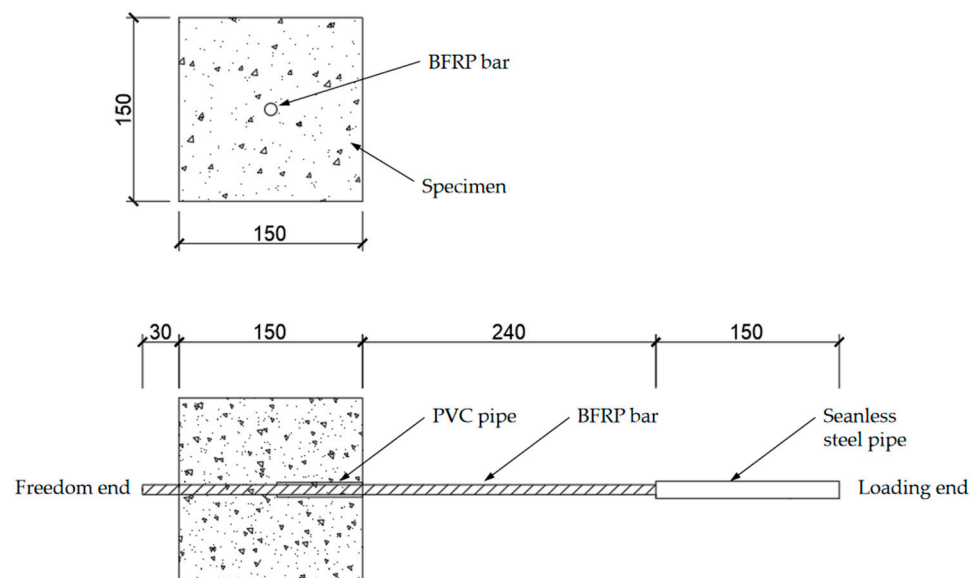


Figure 3. Specimen dimensions.

In this study, pull-out tests were employed to investigate the bonding behavior of BFRP bar-RPC considering the effects of parameters such as fiber volume content (0, 1.5%, 2%) and protective layer thickness (25 mm, 40 mm, 55 mm, 69 mm, the protective layer thickness was achieved by setting eccentric specimens, and because the diameter of the BFRP was 12 mm and the size of the RPC cube test block was 150 mm, and the thickness of the protective layer was 69 mm when the BFRP bar was placed at the center of the RPC cube test block, the thickness of other protective layers was determined based on the distance between the BFRP reinforcement and the centerline of the cube), bond anchorage length of bars ($3d$, $4d$, $5d$; d is the diameter of the bars, the bond length was achieved by adjusting the length of PVC pipe, and the bond length was determined by reference to ACI 440.3R-04 [35]). In addition, a control test was set up to compare the bond strength of BFRP bars in reactive powder concrete (RPC) and normal concrete. Each group had three identical

specimens, so there were 9 groups of 27 specimens for the pull-out test. The casted pull-out specimens are shown in Figure 4.



Figure 4. Pull-out specimens.

2.3. Test Methods

A DDL300 universal testing machine was used for the pull-out test. The upper chuck of the machine was connected to a self-designed loading frame. The top joint of the loading frame was equipped with a freely rotatable ball hinge to ensure that the BFRP bars were always in axial tension during the pull-out test, as shown in Figure 5. The loading frame included upper and lower steel plates and four high-strength screws, and the connections between the upper and lower steel plates and the high-strength screws were fixed by high-strength bolts. The lower steel plate had a large circular hole in the center, and the BFRP bars of the pull-out specimen were extended through the circular hole to the lower chuck of the testing machine.

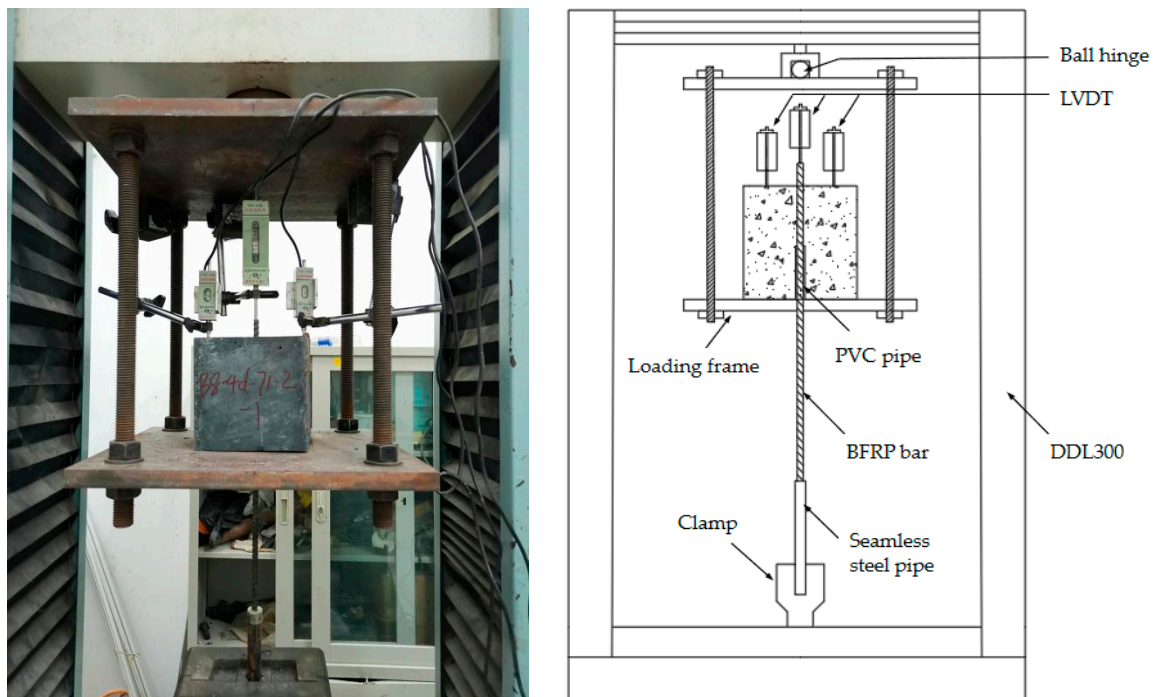


Figure 5. Specimen loading.

The pull-out test was performed under displacement control at a rate of 1 mm/min. Two displacement gauges were symmetrically arranged on the surface of the free end of the concrete block, and one displacement gauge was placed on the free end of the BFRP bar to

measure the relative slip between the BFRP bar and the concrete block. The displacement data and the pull-out load data were collected continuously by fiber optic data acquisition equipment with a frequency of 1 Hz. The test was terminated when one of the following conditions occurred: (1) the concrete block was split; (2) the BFRP bar was pulled off; (3) the displacement of the free end of the BFRP bar reached 20 mm and the load was past the peak.

In practice, the bond stress between BFRP bars and concrete is nonlinearly distributed over the bond length, and the average bond stress over the bond length is adopted as the actual bond stress to simplify the calculation. The bond stresses measured in the bond length range of 5 times the diameter of the reinforcement are relatively uniformly distributed, and it is generally believed that the average bond stress in this range basically reflects the actual bond strength of the specimen. The calculation formula is as follows:

$$\tau = \frac{P}{\pi d l_a} \quad (1)$$

where, d is the diameter of the bars; l_a is the bond anchorage length, P is the pullout load.

3. Experiment Results and Analysis

3.1. Failure Mode

Three failure modes were observed in the pull-out tests: BFRP bar shear failure, concrete splitting failure, and concrete shear failure. As shown in Table 2, BFRP bar shear failure was the primary failure mode, and two different failure processes were observed in the BFRP bar shear failure mode. One kind of pull-out shear failure was that during the pull-out process, the BFRP bar was slowly pulled out and its maximum tensile stress did not reach its ultimate tensile strength, and the concrete did not crack. There was a slight rattling sound, and it was observed that the fibers and resin at the free end of the BFRP bar were delaminated and slid off internally and externally. Eventually, as the pull-out load increased, the slip of the BFRP bar continued to increase, leading to the failure of the bond interface. Another kind of pull-off failure was that the BFRP bar was pulled out slowly at the beginning of the test process, and with the increase in pull-out force, the slip also increased, and the pull-out process was accompanied by a slight sound. When the pull-out force reached the peak load, it turned to decline rapidly, and the decline process was accompanied by a “bang” (the BFRP bar was pulled off). The maximum tensile stress during the test was much less than the ultimate tensile strength of BFRP bars. No cracks appeared on the surface of the concrete block after the test, and the same phenomenon of slippage between the surface layer and the core of the BFRP bars at the free end occurred (see Figure 6a). Splitting the specimens of the two different failure processes mentioned above, it was found that there was a fiber layer of BFRP bars peeling off at the concrete interface. In summary, both types of failure were caused by shear failure of the surface and core of the BFRP bars rather than being pulled apart due to the BFRP bars reaching their ultimate tensile strength.

Table 2. Failure model of specimens.

Specimens Type	Protective Layer Thickness	Bar Diameter	Steel Fiber Dosing	Failure Mode
B12-4d-69-P	69	12	2%	Concrete shear failure
B12-4d-69-2	69	12	2%	BFRP bar shear failure
B12-3d-69-2	69	12	2%	BFRP bar shear failure
B12-5d-69-2	69	12	2%	BFRP bar shear failure
B12-4d-25-2	25	12	2%	BFRP bar shear failure
B12-4d-40-2	40	12	2%	BFRP bar shear failure
B12-4d-55-2	55	12	2%	BFRP bar shear failure
B12-4d-69-0	69	12	0%	Concrete splitting failure
B12-4d-69-1.5	69	12	1.5%	BFRP bar shear failure

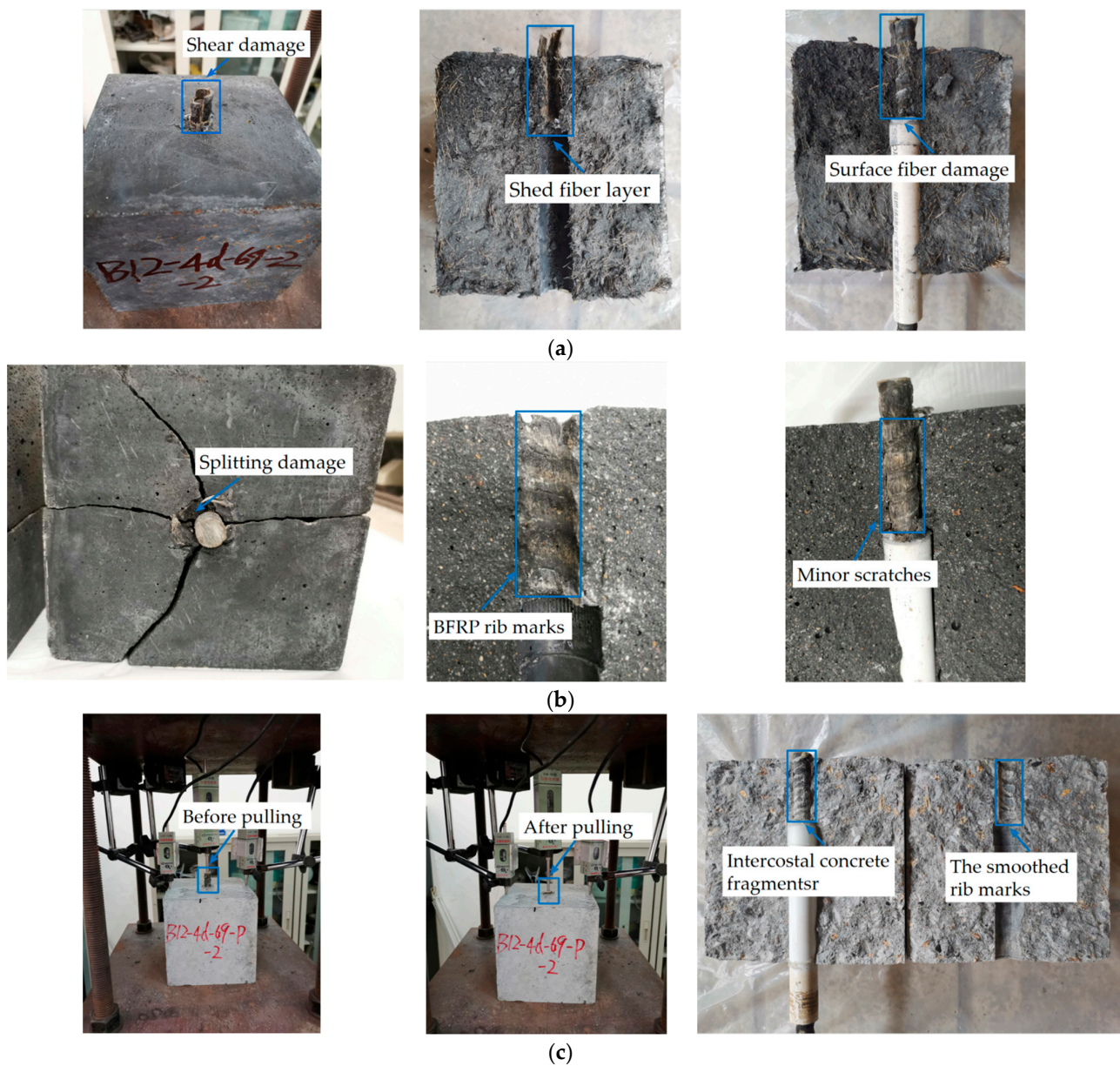


Figure 6. Specimen damage appearance. (a) BFRP bar shear damage. (b) Concrete splitting damage. (c) Concrete shear damage.

For the concrete splitting failure mode, during the ascending stage of the pull-out force, the splitting tensile stress generated by the pull-out force on the concrete exceeded its splitting tensile strength. The concrete block was suddenly split into multiple pieces, and the pull-out force rapidly decreased, as shown in Figure 6b. The splitting failure only occurred in the reactive powder concrete (RPC) specimens with 0% steel fiber content. From the internal interface of the RPC specimen after splitting, it could be observed that there was only slight wear on the surface of the BFRP bars, and there were apparent rib marks of BFRP bars at the concrete interface, which was because the shear stress generated by the pull-out force was relatively small and had not yet reached the bond strength, so the bond interface was relatively well-preserved.

For the concrete shear failure mode, during the shear process, the BFRP bars were slowly pulled out under the pull-out force, the concrete did not split, and the BFRP bars did not reach their ultimate tensile strength, ultimately leading to pull-out failure due to the continuous increase in pull-out force. In the experiment, only the specimens of BFRP bars and ordinary concrete underwent pull-out failure, as shown in Figure 6c. After splitting

the specimen, it could be seen that the hollow area between the ribs of the BFRP bars was filled with concrete fragments, which indicated that shear failure occurred at the concrete interface during the pull-out process, leading to damage of the bonding interface.

In summary, when the convex ribs on the surface of BFRP bars and the concrete between the ribs are subjected to shear force, a shear interface will be formed between the convex ribs or the concrete between the ribs, and the position of the shear interface depends on the relative shear strength of the FRP bars and concrete. Due to the lower shear strength of BFRP bar compared to reactive powder concrete (RPC), the convex ribs of BFRP bar are ground flat or the body of BFRP bar is damaged under shear force, resulting in BFRP bar being pulled out or pulled off and the occurrence of BFRP bar shear failure. When the steel fiber content of reactive powder concrete is 0%, concrete splitting failure occurs before the shear force reaches the shear strength of BFRP bar or reactive powder concrete with 0% steel fiber content. This is because the hardening shrinkage of concrete and the expansion of BFRP bars cause a compression effect between BFRP bars and concrete. During the pulling process, the concrete will be subjected to external tensile stress, while reactive powder concrete without steel fibers has lower tensile strength, resulting in concrete splitting failure. Due to the lower shear strength of ordinary concrete compared to BFRP bars, the concrete at the contact surface is sheared when the bonding interface fails, and the mechanical interlocking effect gradually disappears, ultimately leading to the failure of the bonding interface. So, the bonding interface between BFRP bars and ordinary concrete is subjected to concrete shear failure.

3.2. Effect of Concrete Substrate on Bonding Performance

BFRP bars with 12 mm diameter and 4 d (48 mm) bond length were respectively selected for pull-out tests with plain concrete and reactive powder concrete (RPC) to analyze the difference in bonding performance between the two different concretes. The bonding interface between BFRP bars and reactive powder concrete (RPC) underwent shear failure of BFRP bars, while the bonding interface between BFRP bars and ordinary concrete underwent shear failure of ordinary concrete.

The bond–slip curves of the two failure modes are shown in Figure 7. From the bond–slip curves, it can be seen that: (1) in the micro-slip stage, the two bond–slip curves basically coincide, indicating that the bond strengths of both reactive powder concrete and ordinary concrete with BFRP bar are very close to each other at the early stage of pull-out. (2) The bond–slip curve of BFRP bar and reactive powder concrete had a long upward phase, and the maximum bond strength reached 33 MPa, while the maximum bond strength of BFRP bar and ordinary concrete was about 20 MPa, and the former was about 65% higher than the latter, which was due to the fact that the shear strength of reactive powder concrete is much higher than that of normal concrete, so the BFRP bar and reactive powder concrete had a better bond. (3) The bond–slip curve between BFRP bar and reactive powder concrete reached a peak and then decreased rapidly until it reached 0. This was due to the fact that the BFRP bar reaches the ultimate shear stress and is destroyed by rapid shear, and the interfacial bonding effect is soon lost completely. The bond–slip curve between the BFRP bar and reactive powder concrete in the decreasing stage showed a wave-type resilience decay, which was due to the fact that the concrete interface is destroyed and the concrete debris and the BFRP bar are damaged. The reason is that the concrete interface was destroyed, and the concrete fragments and the BFRP bar formed a new occlusion and friction, until the concrete fragments were completely sheared and the interfacial bond disappeared.

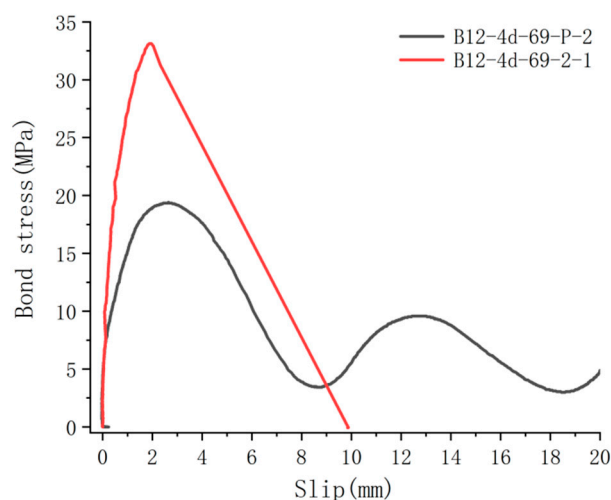


Figure 7. Bond stress–slip curves for different concretes.

From the above comparative analysis, it can also be seen that the BFRP bar and reactive powder (RPC) concrete interface exhibited better bonding performance. Compared with ordinary concrete, the coarse aggregate was removed from the reactive powder concrete (RPC) and replaced by fine sand, which eliminated the micro-cracks caused by the deformation of cement slurry constrained by coarse aggregate and improved the homogeneity of the RPC, thus improving the bond strength. At the same time, the steel fibers mixed in RPC could play the role of crack-blocking enhancement in the specimen, which improved the shear and tensile properties of the concrete, thus improving the bond strength between the BFRP bar and RPC.

3.3. Effect of Steel Fiber Content on Bonding Performance

As can be seen from Table 1, concrete shear failure occurred in the specimens with 0% steel fiber content, and BFRP bar shear failure occurred in the specimens with 1.5% and 2% steel fiber content. The bond–slip curves between BFRP bars and RPC with different steel fiber content are shown in Figure 8a. For the reactive powder concrete (RPC) specimens with 0% steel fiber content, slip occurred between RPC and BFRP bars when the tensile load was small, and the magnitude of the slip load was almost 0. The bond–slip curve had almost no micro-slip phase, indicating that the chemical bond and friction between the BFRP bar and RPC were very small. The ascending section of the bond–slip curve varied approximately linearly, and the amount of slip grew faster. When the bond stress was 15 MPa, the slip amount reached 2 mm. This indicates that the bond strength was weak, especially the mechanical interlocking effect. When steel fibers were added to the reactive powder concrete (RPC), the bond strength of BFRP bars and reactive powder concrete (RPC) was significantly enhanced. The slip load was 2.5 MPa when the steel fiber content was 1.5%, and the slip load could reach more than 10 MPa when the steel fiber content was 2%. It can be seen that the incorporation of steel fibers can significantly limit the development of slip of BFRP bars and enhance the synergistic working performance of BFRP bars and reactive powder concrete (RPC).

Adding steel fibers to reactive powder concrete (RPC) can also affect the bond strength between BFRP bars and reactive powder concrete (RPC), as shown in Figure 8b. The bond strength of the reactive powder concrete (RPC) specimen with 0% steel fiber content was only 24.2 MPa, while the bond strength of the RPC specimen with 2% content was 34.5 MPa, and the latter was 42.5% higher than the former. The ultimate bond stress was also increased with the increase in fiber content from 1.5% to 2%. The specimens with 0% steel fiber content underwent concrete splitting failure and, therefore, the bond strength was smaller, which failed to fully reflect the bonding performance of the interface between BFRP bars and reactive powder concrete (RPC). The addition of steel fibers to the reactive powder concrete (RPC) can delay or prevent the occurrence and development of concrete cracks

and improve the tensile strength of concrete, thus making full use of the performance of the bonding interface. Therefore, the addition of steel fibers to the reactive powder concrete (RPC) also has a significant enhancement effect on the bond strength of BFRP bars and reactive powder concrete (RPC).

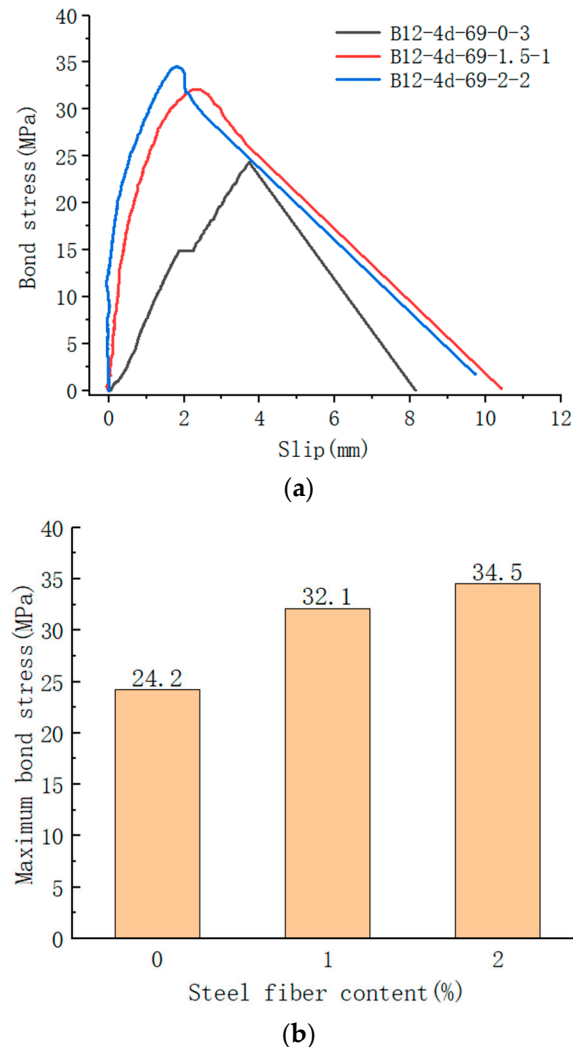


Figure 8. Effect of fiber content on bonding performance. (a) Bond stress–slip curves for different steel fiber contents. (b) Average bond strengths of different steel fiber contents.

3.4. Effect of Bond Anchorage Length on Bonding Performance

BFRP bars of 12 mm diameter were selected, and three bond anchorage lengths of 3 d, 4 d, and 5 d (d is the diameter of the bars) were set to study the effect of bond anchorage length on the bond strength of BFRP bars and reactive powder concrete (RPC), and the bond slip curves are shown in Figure 9. BFRP bar shear failure occurred in all specimens with three bond lengths, and the corresponding bond–slip curves all had the micro-slip phase, slip-rise phase, and decline phase, but only the bond–slip curve with bond length 3 d still had the residual stress phase. The reason may be that the specimens with 4 d and 5 d bond lengths were damaged by the pullout of the BFRP bar, and the load was rapidly reduced to 0 kN. The specimens with 3 d bond lengths were damaged by the pullout of the BFRP bar, and the residual friction and mechanical occlusion of the shear surface of the bar still existed in the pullout process.

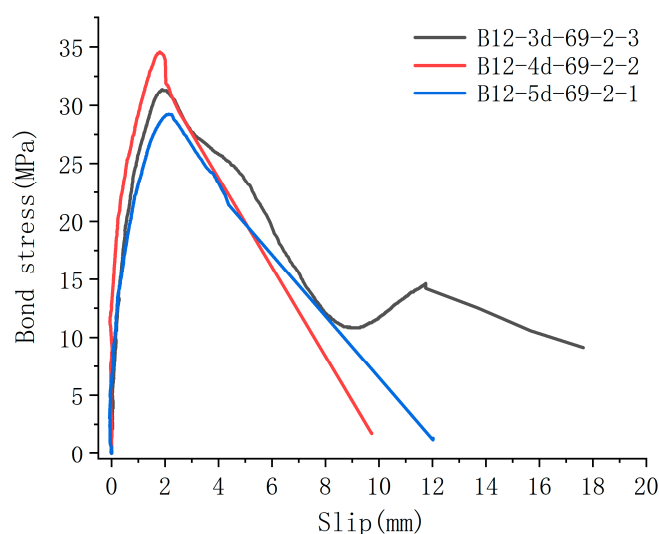


Figure 9. Bond stress–slip curves for different bond lengths.

All three bond anchorage lengths of specimens reached the ultimate bond strength at a slip of about 2 mm. The ultimate bond strengths for bond lengths of 3 d, 4 d, and 5 d were 32 MPa, 35 MPa, and 29 MPa, respectively. With the increase in bond length, the ultimate bond strength tended to increase first and then decrease. However, according to Hossain's studies [36], the bond strength decreases with increasing bond length. The opposite occurred in this test when the bond length of 3 d was increased to 4 d, which may be related to the failure process. The specimen with a bond length of 3 d underwent pull-out shear failure, and the inner and outer delamination of the BFRP bar slipped off much earlier, which resulted in a smaller bond strength. It is inferred that BFRP bars and RPC may have an optimal bond length to maximize the ultimate bond strength, and the bond strength will decrease with the increase in bond length when the bond length is greater than the optimal bond length.

3.5. Effect of Protective Layer Thickness on Bonding Performance

In this test, four different protective layer thicknesses of 25 mm, 40 mm, 55 mm, and 69 mm were set for BFRP bars of 12 mm diameter and 4 d bond length to investigate the influence of protective layer thickness on bonding performance. All of the above specimens experienced BFRP bar shear failure, and the specimens with a protective layer thickness of 69 mm showed pull-out shear failure, while the specimens with 25 mm, 40 mm, and 55 mm protective layers had both pull-out shear failure and pull-off failure processes in each group.

The bond–slip curves of different protective film thicknesses are shown in Figure 10, from which it can be seen that the bond–slip curves corresponding to different protective film thicknesses basically followed a similar law, i.e., they first passed through the microslip phase, the slip phase and the decline phase in turn. As the thickness of the protective layer increased, the microslip phase of the bond–slip curve became longer, and the slip phase also basically showed a larger slope, i.e., it had a stronger bond, which was due to the fact that the larger the protective layer, the greater the shrinkage of the concrete, which increased the friction effect and the mechanical occlusion effect. It has been pointed out that too thin a protective layer would lead to concrete splitting damage at the interface, but the above specimen failures were all BFRP reinforcement shear damage, indicating that a protective layer thickness of 25 mm was able to fully utilize the bonding properties of the reinforcement and RPC.

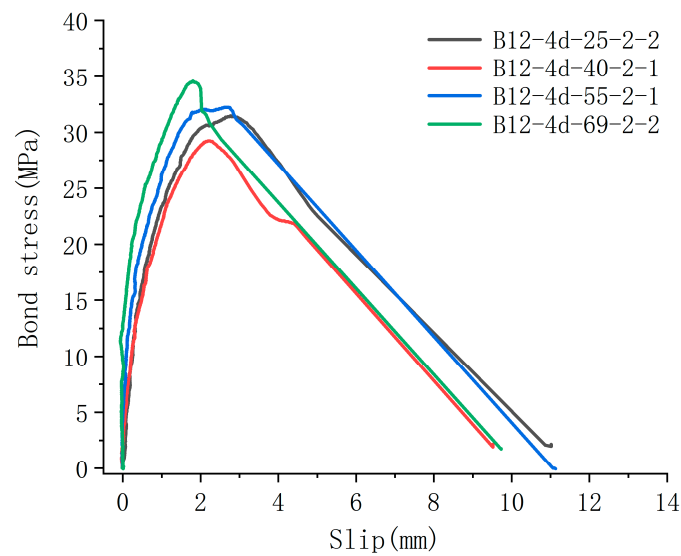


Figure 10. Bond stress–slip curves for different protective layer thicknesses.

With the increase in the protective layer thickness, the bond strength of BFRP bar and reactive powder concrete (RPC) had basically improved to a certain extent, but the improvement effect was not very significant. For example, as shown in Figure 11, when the thickness of the protective layer was increased from 25 mm (corresponding to a bond strength of 31.47 MPa) to 55 mm (corresponding to a bond strength of 32.23 MPa), the bond strength increased by only 2.4%. When the thickness of the protective layer was increased from 55 mm (corresponding to a bond strength of 32.23 MPa) to 69 mm (corresponding to a bond strength of 34.58 MPa), the bond strength only increased by 7%. From this, it can be seen that changing the thickness of the protective layer has little effect on the bonding performance between BFRP bars and reactive powder concrete (RPC). The reason for this is that the hardening shrinkage of reactive powder concrete was smaller compared to that of ordinary concrete, and therefore, the increase in the thickness of the protective layer had little effect on the extrusion between the BFRP reinforcement and the RPC, so the bond strength was not improved.

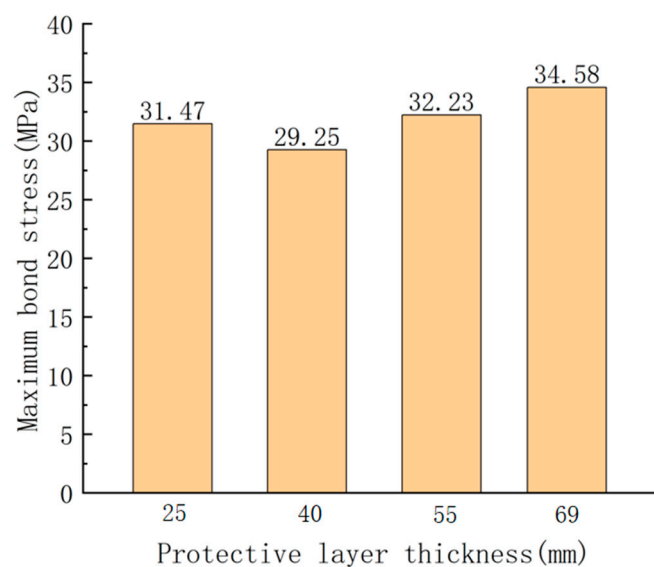


Figure 11. Average bond strengths for different protective layer thicknesses.

4. Conclusions

Three failure modes were observed in the pull-out tests: BFRP bar shear failure, splitting failure, and concrete shear failure. The failure mode depended on the relative shear strength of BFRP bar and matrix. BFRP shear failure occurred at the interface between BFRP bar and reactive powder concrete (RPC). However, the interface between BFRP bar and ordinary concrete underwent concrete shear failure. At the same time, the tensile performance of the matrix also affected the failure mode, for example, the splitting failure only occurred in the reactive powder concrete (RPC) specimens with 0% steel fiber content. Only the specimens of BFRP bars and ordinary concrete underwent pull-out failure. The other specimens experienced BFRP bar shear failure.

The bond strength between BFRP bars and reactive powder concrete (RPC) is much greater than that between BFRP bars and ordinary concrete, which indicates that BFRP bars have excellent bonding performance with reactive powder concrete (RPC) and broad engineering application prospects. This is because adding a certain amount of steel fiber into the RPC can play a role in crack resistance and enhance the tensile capacity of the concrete, thus improving the bond strength.

Adding steel fibers to reactive powder concrete can change the failure mode of the interface and enhance the friction and mechanical bite between the interfaces. The bond strengths of BFRP bars and reactive powder concrete (RPC) with 0%, 1.5%, and 2% steel fiber content were 24.2 MPa, 32.1 MPa, and 34.5 MPa, respectively. The addition of steel fibers to the reactive powder concrete (RPC) also has a significant enhancement effect on the bond strength of BFRP bars and reactive powder concrete (RPC), and the bond strength increases with the increase in steel fiber content.

With the increase in bond anchorage length, the ultimate bond strength showed a tendency to increase first and then decrease. There may be an optimal bonding length between BFRP bar and reactive powder concrete, and when the optimal bonding length is exceeded, the bond strength decreases with the increase in bonding length.

With the increase in the protective layer thickness, the bond strength of BFRP bar and reactive powder concrete (RPC) basically improved to a certain extent, but the improvement effect was not very significant. A protective layer thickness of 25 mm can already provide effective bond strength for BFRP bars and reactive powder concrete (RPC).

Therefore, the bonding performance between BFRP bar and reactive powder concrete can be adjusted by changing the steel fiber parameters, bonding length, and protective layer thickness.

Author Contributions: J.X., K.Z., L.L. and H.J. contributed to the design of the manuscript. Y.M. and X.C. carried out data collection and processing. L.L., Y.M., X.C., L.H., G.W. and X.C. were involved in casting the specimens. J.X., L.L., Y.M. and H.J. wrote and revised the paper. All authors have read and agreed to the published version of the manuscript.

Funding: The authors appreciate the financial support provided by the National Natural Science Foundation of China with Grant No. 52278160 and Grant No. 51808133, the Innovation Project of Guangdong Graduate Education with Grant No. 2019JGXM101, Young innovative talents project of regular universities in Guangdong Province with Grant No. 2018KQNCX278, and Guangdong Basic and Applied Basic Research Foundation with Grant No. 2020A1515110814 and Grant No. 2023A1515012081.

Data Availability Statement: The data that support the findings of this study are available from the corresponding author upon reasonable request.

Acknowledgments: The authors would like to thank all of the anonymous referees for their constructive comments and suggestions. The authors gratefully acknowledge the laboratory of School of Civil and Transportation Engineering, Guangdong University of Technology for providing the resources required for this study.

Conflicts of Interest: The authors declare no conflict of interest.

References

1. Jiang, H.B.; Huang, C.W.; Mei, G.Y.; Gao, X.J.; Tian, Y.Q.; Sun, X.D. Experimental and numerical investigations on direct shear performance of UHPC dry joints. *Eng. Struct.* **2023**, *283*, 115872. [[CrossRef](#)]
2. Feng, J.H.; Li, P.S.; Wu, J.P.; Jiang, H.B.; Tian, Y.Q.; Sun, X.D. Shear behavior of externally prestressed UHPC beams without stirrups. *Case Stud. Constr. Mater.* **2023**, *18*, e01766. [[CrossRef](#)]
3. Xiao, J.; Qu, W.J.; Li, W.G.; Zhu, P. Investigation on effect of aggregate on three non-destructive testing properties of concrete subjected to sulfuric acid attack. *Constr. Build. Mater.* **2016**, *115*, 486–495. [[CrossRef](#)]
4. Xiao, J.; Huang, H.; Zeng, H.; Liu, L.; Li, L.; Jiang, H.; Zhong, Z.; Chen, A. Experimental Study on the Sulfuric Acid Corrosion Resistance of PHC Used for Pipe Pile and NSC Used in Engineering. *Buildings* **2023**, *13*, 1596. [[CrossRef](#)]
5. Zhang, W.P.; Chen, H.; Gu, X.L. Tensile behaviour of corroded steel bars under different strain rates. *Mag. Concr. Res.* **2016**, *68*, 127–140. [[CrossRef](#)]
6. Ying, J.W.; Wang, W.B.; Xiao, J.Z. Chloride diffusion in concrete with carbonated recycled coarse aggregates under biaxial compression. *Front. Struct. Civ. Eng.* **2023**, *17*, 637–648. [[CrossRef](#)]
7. Shao, W.; Nie, Y.H.; Liang, F.Y.; Shi, D.D. A novel comprehensive evaluation method for the corrosion initiation life of RC hollow piles in chloride environments. *Constr. Build. Mater.* **2020**, *249*, 118801. [[CrossRef](#)]
8. Li, L.; Gong, W.B.; Li, J.P. Prediction on service life of concrete pipeline buried in chlorinated environment under nonuniformly distributed earth pressure. *Constr. Build. Mater.* **2020**, *243*, 118162. [[CrossRef](#)]
9. Lu, Z.H.; Wu, S.Y.; Tang, Z.; Zhao, Y.G.; Li, W.G. Effect of chloride-induced corrosion on the bond behaviors between steel strands and concrete. *Mater. Struct.* **2021**, *54*, 129. [[CrossRef](#)]
10. Fu, B.; Liu, K.C.; Chen, J.F.; Teng, J.G. Concrete reinforced with macro fibres recycled from waste GFRP. *Constr. Build. Mater.* **2021**, *310*, 125063. [[CrossRef](#)]
11. Wang, Y.; Li, X.D.; Li, J.H.; Wang, Q.; Xu, B.; Deng, J. Debonding damage detection of the CFRP-concrete interface based on piezoelectric ceramics by the wave-based method. *Constr. Build. Mater.* **2019**, *210*, 514–524. [[CrossRef](#)]
12. Xian, G.; Guo, R.; Li, C.; Hong, B. Mechanical properties of carbon/glass fiber reinforced polymer plates with sandwich structure exposed to freezing-thawing environment: Effects of water immersion, bending loading and fiber hybrid mode. *Mech. Adv. Mater. Struct.* **2023**, *30*, 814–834. [[CrossRef](#)]
13. Wu, J.Y.; Zhu, Y.Q.; Li, C.G. Experimental Investigation of Fatigue Capacity of Bending-Anchored CFRP Cables. *Polymers* **2023**, *15*, 2483. [[CrossRef](#)] [[PubMed](#)]
14. Xie, J.H.; Li, Y.C.; Lu, Z.Y.; Fan, Z.H.; Li, J.L.; Li, S.X. Effects of Immersion in Water, Alkaline Solution, and Seawater on the Shear Performance of Basalt FRP Bars in Seawater-Sea Sand Concrete. *J. Compos. Constr.* **2022**, *26*, 04021071. [[CrossRef](#)]
15. Zhou, J.Y.; Wang, X.; Peng, Z.Q.; Wu, Z.S.; Zhu, Z.G. Failure mechanism and optimization of fiber-reinforced polymer cable-anchor system based on 3D finite element model. *Eng. Struct.* **2021**, *243*, 112664. [[CrossRef](#)]
16. Wang, X.; Liu, S.; Shi, Y.W.; Wu, Z.S.; He, W.D. Integrated High-Performance Concrete Beams Reinforced with Hybrid BFRP and Steel Bars. *J. Struct. Eng.* **2022**, *148*, 04021235. [[CrossRef](#)]
17. Wu, G.; Dong, Z.Q.; Wang, X.; Zhu, Y.; Wu, Z.S. Prediction of Long-Term Performance and Durability of BFRP Bars under the Combined Effect of Sustained Load and Corrosive Solutions. *J. Compos. Constr.* **2015**, *19*, 04014058. [[CrossRef](#)]
18. Lu, Z.Y.; Li, W.K.; Zeng, X.Y.; Pan, Y.F. Durability of BFRP bars and BFRP reinforced seawater sea-sand concrete beams immersed in water and simulated seawater. *Constr. Build. Mater.* **2023**, *363*, 129845. [[CrossRef](#)]
19. Zhu, P.; Mao, X.Q.; Qu, W.J.; Li, Z.Y.; Ma, Z.J. Investigation of using recycled powder from waste of clay bricks and cement solids in reactive powder concrete. *Constr. Build. Mater.* **2016**, *113*, 246–254. [[CrossRef](#)]
20. Mao, X.Q.; Qu, W.J.; Zhu, P.; Xiao, J.Z. Influence of recycled powder on chloride penetration resistance of green reactive powder concrete. *Constr. Build. Mater.* **2020**, *251*, 119049. [[CrossRef](#)]
21. Feng, J.; Fang, S.; Chen, M.; Fang, Z.; Liang, W. Effect of joint width on shear behaviour of wet joints using reactive powder concrete with confining stress. *Eng. Struct.* **2023**, *293*, 116566. [[CrossRef](#)]
22. Wang, Z.K.; Zhao, X.L.; Xian, G.J.; Wu, G.; Raman, R.K.S.; Al-Saadi, S. Effect of sustained load and seawater and sea sand concrete environment on durability of basalt- and glass-fibre reinforced polymer (B/GFRP) bars. *Corros. Sci.* **2018**, *138*, 200–218. [[CrossRef](#)]
23. Xiong, Z.; Wei, W.; Liu, F.; Cui, C.Y.; Li, L.J.; Zou, R.; Zeng, Y. Bond behaviour of recycled aggregate concrete with basalt fibre-reinforced polymer bars. *Compos. Struct.* **2021**, *256*, 113078. [[CrossRef](#)]
24. Trabacchin, G.; Sebastian, W.; Zhang, M.Z. Experimental and analytical study of bond between basalt FRP bars and geopolymer concrete. *Constr. Build. Mater.* **2022**, *315*, 125461. [[CrossRef](#)]
25. Ahmed, S.A.S.; Fahmy, M.F.M.; Wu, Z.S. Experimental Study and Numerical Modeling of Cyclic Bond-Slip Behavior of Basalt FRP Bars in Concrete. *J. Compos. Constr.* **2018**, *22*, 04018050. [[CrossRef](#)]
26. Henin, E.; Tawadrous, R.; Morcou, G. Effect of surface condition on the bond of Basalt Fiber-Reinforced Polymer bars in concrete. *Constr. Build. Mater.* **2019**, *226*, 449–458. [[CrossRef](#)]
27. Junyan, D.; Shiping, Y.; Fengjuan, L.; Pengjie, D. Study on bond performance between seawater sea-sand concrete and BFRP bars under chloride corrosion. *Constr. Build. Mater.* **2023**, *371*, 130718. [[CrossRef](#)]
28. Chen, W.X.; Meng, F.J.; Sun, H.; Guo, Z.K. Bond behaviors of BFRP bar-to-concrete interface under dynamic loading. *Constr. Build. Mater.* **2021**, *305*, 124812. [[CrossRef](#)]

29. Lu, Z.Y.; Su, L.Z.; Lai, J.W.; Xie, J.H.; Yuan, B. Bond durability of BFRP bars embedded in concrete with fly ash in aggressive environments. *Compos. Struct.* **2021**, *271*, 114121. [[CrossRef](#)]
30. Sun, X.Y.; Gao, C.; Wang, H.L. Bond performance between BFRP bars and 3D printed concrete. *Constr. Build. Mater.* **2021**, *269*, 121325. [[CrossRef](#)]
31. Wang, D.H.; Han, L.; Ju, Y.Z.; Zeng, C.; Li, Z.Y. Bond behavior between reinforcing bar and reactive powder concrete. *Struct. Concr.* **2022**, *23*, 2630–2642. [[CrossRef](#)]
32. Piccinini, A.C.; da Silva, L.C.P.; Campos, A. Bond of Reinforcement in Reactive Powder Concrete a Different Ages. *ACI Mater. J.* **2021**, *118*, 169–176. [[CrossRef](#)]
33. Bae, B.I.; Choi, H.K.; Choi, C.S. Bond stress between conventional reinforcement and steel fibre reinforced reactive powder concrete. *Constr. Build. Mater.* **2016**, *112*, 825–835. [[CrossRef](#)]
34. GB/T 30022-2013; Test Method for Basic Mechanical Properties of Fiber Reinforced Polymer Bar. Standards Press of China: Beijing, China, 2013.
35. ACI Committee 440. *Guide Test Methods for Fiber-Reinforced Polymers (FRPs) for Reinforcing or Strengthening Concrete Structures*; American Concrete Institute: Detroit, MI, USA, 2004.
36. Hossain, K.M.A.; Ametrano, D.; Lachemi, M. The bond between glass-fibre-reinforced polymer bars and ultra-high-strength concrete. *Proc. Inst. Civ. Eng.-Constr. Mater.* **2018**, *171*, 161–176. [[CrossRef](#)]

Disclaimer/Publisher’s Note: The statements, opinions and data contained in all publications are solely those of the individual author(s) and contributor(s) and not of MDPI and/or the editor(s). MDPI and/or the editor(s) disclaim responsibility for any injury to people or property resulting from any ideas, methods, instructions or products referred to in the content.